Edinburgh 99/8
CERN-TH/99-253
hep-lat/9908041

August 1999

THE SPECTRUM OF THE THREE-DIMENSIONAL ADJOINT HIGGS MODEL AND HOT SU(2) GAUGE THEORY

A. Hart[a] and O. Philipsen[b]

[a] *Department of Physics and Astronomy, University of Edinburgh, Edinburgh EH9 3JZ, Scotland, UK*

[b] *Theory Division, CERN, CH-1211 Geneva 23, Switzerland*

Abstract. We compute the mass spectrum of the SU(2) adjoint Higgs model in $2+1$ dimensions at several points located in the (metastable) confinement region of its phase diagram. We find a dense spectrum consisting of an almost unaltered repetition of the glueball spectrum of the pure gauge theory, and additional bound states of adjoint scalars. For the parameters chosen, the model represents the effective finite temperature theory for pure SU(2) gauge theory in four dimensions, obtained after perturbative dimensional reduction. Comparing with the spectrum of screening masses obtained in recent simulations of four-dimensional pure gauge theory at finite temperature, for the low lying states we find quantitative agreement between the full and the effective theory for temperatures as low as $T = 2T_c$. This establishes the model under study as the correct effective theory, and dimensional reduction as a viable tool for the description of thermodynamic properties. We furthermore compare the perturbative contribution $\sim gT$ with the non-perturbative contributions $\sim g^2T$ and $\sim g^3T$ to the Debye mass. The latter turns out to be dominated by the scale g^2T, whereas higher order contributions are small corrections.

PACS numbers: 12.38.Gc, 11.10.Wx, 12.38.Mh, 11.10.Kk, 14.80.Cp.
Keywords: dimensional reduction, quark gluon plasma, Debye mass.

CERN-TH/99-253
August 1999

1 Introduction

The thermodynamic properties of non-Abelian field theories at finite temperature are known to be non-perturbative due to the confining nature of the Matsubara zero mode sector. Lattice simulations of the full problem are numerically expensive and especially difficult if fermions are present. A way to circumvent both problems is to perturbatively integrate out the non-zero Matsubara and momentum modes of order $\sim T$ and higher to arrive at a purely bosonic, three-dimensional effective theory describing the static quantities of the original theory [1]. Three-dimensional gauge theories are non-perturbative, but readily accessible by lattice simulations. This programme has been successfully carried out in studies of the electroweak phase transition, where the phase structure and nature of the transition were computed from the dimensionally reduced theory, both by numerical [2] and analytical [3] methods. The results have been found to agree to remarkable accuracy with the answers obtained recently from four-dimensional simulations [4].

In view of the experimental search for the quark gluon plasma in heavy ion collisions at RHIC and LHC it is of particular interest to see to what extent this programme can be carried over to QCD. The reduction step for a SU(N) gauge theory with N_f flavours of fermions has been carried out to two loops in [5] (see also [6]). The effective theory obtained in this case is a three-dimensional SU(N) adjoint Higgs theory, with the scalars corresponding to the electric gauge potential, A_0, in the unreduced theory. In the framework of dimensional reduction N_f only modifies the parameters of the effective, bosonic theory. To be specific, and to compare with existing four-dimensional work, we discuss in this study the simplest case of $N_f = 0, N = 2$.

Simulations of the three-dimensional SU(2) adjoint Higgs model revealed that this theory has a phase diagram with continuously connected Higgs and confinement regions [7, 5], which are partially separated by a line of first order phase transitions. This is in contrast to the four-dimensional SU(2) Yang-Mills theory at finite T, which displays a second order phase transition [8]. Hence the deconfinement phase transition cannot be described by the effective theory. Based on the apparent convergence properties of the reduction step, however, it has been argued [5] that the effective theory still yields the correct description of static correlation functions at temperatures sufficiently above the critical temperature, T_c, and hence valuable information about the plasma state.

In recent publications [9, 10] it was established that dimensional reduction indeed works in the sense that the spectrum measured in four-dimensional simulations at finite temperature can be classified by the symmetry group of a purely three-dimensional theory. This does not yet determine the precise form of the effective theory. Earlier simulations of the SU(2) adjoint Higgs model have concluded it to be a good effective theory by comparing the static potential [11] and gauge-fixed propagators [12] between the full and the effective theory. The question of the dynamical rôle of the A_0 and whether there is a further hierarchy $gT \ll g^2T$ in the reduced theory, however, is still not precisely answered. The purpose of the present paper is to quantitatively test

the agreement of a wide range of gauge-invariant correlation functions between the full and the effective theory at temperatures not much larger than the critical temperature. We compute correlation functions of the three-dimensional SU(2) adjoint Higgs model on the lattice and extract the corresponding screening masses for various quantum number channels. These are then compared with the four-dimensional calculation of finite temperature SU(2) Yang-Mills theory in [10]. We find indeed that dimensional reduction works remarkably well, even at the quantitative level. Furthermore, we are able to identify the lightest gauge-invariant state to consist of A_0, which hence may not be integrated out.

The continuum action of the SU(2) adjoint Higgs model is given by

$$S = \int d^3x \left\{ \frac{1}{2}\mathrm{Tr}\,(F_{ij}F_{ij}) + \mathrm{Tr}\,(D_i\varphi D_i\varphi) + m_3^2\mathrm{Tr}\,(\varphi\varphi) + \lambda_3(\mathrm{Tr}\,(\varphi\varphi))^2 \right\}, \qquad (1)$$

where $F_{ij} = \partial_i A_j - \partial_j A_i + ig[A_i, A_j]$, $D_i\varphi = \partial_i\varphi + ig_3[A_i, \varphi]$ and F_{ij}, A_i, and φ are all traceless 2×2 Hermitian matrices ($\varphi = \varphi^a\sigma_a/2$, *etc.*). The physical properties of the theory are fixed by the two dimensionless ratios

$$x = \frac{\lambda_3}{g_3^2}, \quad y = \frac{m_3^2}{g_3^4}. \qquad (2)$$

In the framework of dimensional reduction these parameters are completely determined by the four-dimensional gauge coupling, g^2, and the temperature, T. Since g^2 is a running coupling its value is in turn fixed by a renormalisation scale $\Lambda_{\overline{\mathrm{MS}}}$. The details of the derivation of x, y to two loops can be found in [5]. Here we merely quote the results to furnish the connection between the three-dimensional parameters and the four-dimensional, finite T situation. Choosing the renormalisation scale as in [5] and expressing $\Lambda_{\overline{\mathrm{MS}}}$ through the critical temperature as measured on the lattice [8], $T_c = 1.23(11)\Lambda_{\overline{\mathrm{MS}}}$, one has

$$g_3^2 = \frac{10.7668}{\ln(8.3T/T_c)}T, \quad x = \frac{0.3636}{\ln(6.6T/T_c)}, \quad y(x) = \frac{2}{9\pi^2 x} + \frac{1}{4\pi^2} + \mathcal{O}(x). \qquad (3)$$

With these equations, specifying T/T_c completely fixes the parameters x, y of the reduced model.

In this paper we study specifically the temperatures $T = 2T_c$, $T = 4T_c$ and $T = 5T_c$ (with the corresponding values of x and y given in Table 1). Note, however, that these parameters lie in the Higgs phase of the model, whereas the connection to four dimensional physics is only valid in the confinement phase [13, 5]. The dimensional reduction programme would be futile were it not that the confinement phase is metastable in this region of the phase diagram. Starting with a configuration in the confinement phase, we may re-thermalise and make many measurements at the appropriate parameters before a tunnelling transition occurs to the Higgs phase. In practice, the phases are so strongly separated that no tunnelling occurred in our simulations.

In order to discuss correlation functions of the effective theory, it is most convenient to ignore the finite T context and to discuss the properties of the $2+1$ dimensional Higgs model by itself, as we shall do in the following two sections. This will also enable us to compare the dynamics of the SU(2) adjoint Higgs model in its confining phase with that of the $2+1$ dimensional pure gauge theory and fundamental Higgs model, whose spectra are known in some detail [14, 15], and thus to learn about some general features of three-dimensional confinement. In Sec. 2 we introduce the corresponding lattice action, the operators considered and some technical details about our numerical simulation. In Sec. 3 we present our detailed numerical results for the spectrum of the model, including checks for finite size effects and a numerical continuum extrapolation. Then we return in Sec. 4 to an interpretation and discussion of our results in the context of finite temperature pure gauge theory, before giving our conclusions.

2 Lattice methods

2.1 Action and parameters

The discretised form of the action (1), with leading order lattice spacing corrections of $\mathcal{O}(a)$, is

$$\begin{aligned} S &= \beta \sum_{x,i>j} \left(1 - \frac{1}{2}\mathrm{Tr}\, U_{ij}(x)\right) + 2\sum_x \mathrm{Tr}\left(\varphi(x)\varphi(x)\right) \\ &- 2\kappa \sum_{x,\mu} \mathrm{Tr}\left(\varphi(x) U_\mu(x) \varphi(x+\hat{\mu}a) U^\dagger(x)\right) + \lambda \sum_x (2\mathrm{Tr}\left(\varphi(x)\varphi(x)\right) - 1)^2. \end{aligned} \quad (4)$$

(The lattice scalar field has been rescaled relative to the continuum.) The parameters of the continuum and lattice theory are up to two loops related by a set of equations specifying the lines of constant physics in the lattice parameter space $\{\beta, \kappa, \lambda\}$ [16],

$$\begin{aligned} \beta &= \frac{4}{a g_3^2}, \quad \lambda = \frac{x\kappa^2}{\beta}, \\ y &= \frac{\beta^2}{8}\left(\frac{1}{\kappa} - 3 - \frac{2x\kappa}{\beta}\right) + \frac{\Sigma\beta}{4\pi}\left(1 + \frac{5}{4}x\right) \\ &+ \frac{1}{16\pi^2}\left[(20x - 10x^2)\left(\ln\left(\frac{3\beta}{2}\right) + 0.09\right) + 8.7 + 11.6x\right]. \end{aligned} \quad (5)$$

where $\Sigma = 3.17591$. For a given pair of continuum parameters x, y these equations determine the lattice parameters κ, λ as a function of lattice spacing, and hence govern the approach to the continuum limit, $\beta \to \infty$. It is along such trajectories that we should observe a scaling of dimensionful quantities such as the masses. Due to superrenormalisability of the theory, the above perturbative relation is exact in the continuum limit. Based on previous experience [7] we expect it to be accurate for all

$\beta > 6$. As a consequence of the presence of scalar fields in the action, the leading order lattice spacing corrections to mass ratios should be linear in a.

2.2 Blocking of fields

Since we work in the confinement region of the theory, the physical states are expected to be bound states, which are spatially extended. In order to improve the projection of any operator onto such states, it is necessary to smear the operators in the spatial plane so that their extension becomes comparable to the size of the states. This can be achieved by using "blocked" field variables instead of the elementary ones in the expressions for the operators. We use blocked link variables at blocking level n as proposed in [17],

$$\begin{aligned} U_i^{(n)}(x) &= \frac{1}{3}\Big\{U_i^{(n-1)}(x)U_i^{(n-1)}(x+\hat{i}) \\ &\quad + \sum_{j=\pm 1, j\neq i}^{\pm 2} U_j^{(n-1)}(x)U_i^{(n-1)}(x+\hat{j})U_i^{(n-1)}(x+\hat{i}+\hat{j})U_j^{(n-1)\dagger}(x+2\hat{i})\Big\}. \end{aligned} \quad (6)$$

For the scalars, we adapt the procedure employed in [15] to the case of adjoint fields,

$$\begin{aligned} \varphi^{(n)}(x) &= \frac{1}{5}\Bigg\{\varphi^{(n-1)}(x) + \sum_{j=1}^{2}\Big[U_j^{(n-1)}(x)\varphi^{(n-1)}(x+\hat{\jmath})U_j^{(n-1)\dagger}(x) \\ &\qquad + U_j^{(n-1)\dagger}(x-\hat{\jmath})\varphi^{(n-1)}(x-\hat{\jmath})U_j^{(n-1)}(x-\hat{\jmath})\Big]\Bigg\}\ . \end{aligned} \quad (7)$$

Note that we will take correlations in the $\hat{3}$ direction and so our blocking always remains within the $(1,2)$-plane to avoid spoiling the transfer matrix of the theory and the positivity properties of the correlation functions. In addition, we consider blocked scalar fields $\varphi^{(n,j)}(x)$ with non-local contributions from one spatial direction j only:

$$\begin{aligned} \varphi^{(n,j)}(x) = \frac{1}{3}\Big\{\varphi^{(n-1,j)}(x) &+ U_j^{(n-1)}(x)\varphi^{(n-1,j)}(x+\hat{\jmath})U_j^{(n-1)\dagger}(x)) \\ &+ U_j^{(n-1)\dagger}(x-\hat{\jmath})\varphi^{(n-1,j)}(x-\hat{\jmath})U_j^{(n-1)}(x-\hat{\jmath})\Big\},\ j=1,2. \end{aligned} \quad (8)$$

2.3 Basic operators

The operators we use in our simulations are constructed from several basic gauge-invariant operator types, which we now list before specifying the quantum numbers. We have operators involving only scalar fields or products of scalar and gauge field variables,

$$R(x) = \mathrm{Tr}\,(\varphi^2(x))$$

$$
\begin{aligned}
L_i(x) &= \mathrm{Tr}\,\Big(\varphi(x)U_i(x)\varphi(x+\hat{\imath})U_i^\dagger(x)\Big) \\
A_{ij}^+(x) &= \mathrm{Tr}\,\Big(U_i(x)U_i(x+\hat{\imath})\varphi(x+2\hat{\imath})U_i^\dagger(x+\hat{\imath})U_i^\dagger(x)U_j(x)\varphi(x+\hat{\jmath})U_j^\dagger(x)\Big) \qquad (9) \\
A_{ij}^-(x) &= \mathrm{Tr}\,\Big(U_i(x)U_i(x+\hat{\imath})\varphi(x+2\hat{\imath})U_i^\dagger(x+\hat{\imath})U_i^\dagger(x)U_j(x)\varphi(x+\hat{\jmath})U_j^\dagger(x)\varphi(x)\Big)\,.
\end{aligned}
$$

Other mixed operators are

$$
\begin{aligned}
B_{||}(x) &= \mathrm{Tr}\,(\varphi(x)U_{ij}(x)), \\
B_\perp(x) &= \left[\mathrm{Tr}\,T^a\left(U_{ij}(x)-\varphi(x)\frac{\mathrm{Tr}\,(\varphi(x)U_{ij}(x))}{\sqrt{\mathrm{Tr}\,(\varphi^2(x))}}\right)\right]^2 . \qquad (10)
\end{aligned}
$$

The naming of the operators becomes apparent when considering the continuum limit, in which $B_{||}(x) \sim \mathrm{Tr}\,(\varphi(x)F_{ij}(x))$ gives the projection of the field strength along the scalar field and $B_\perp(x)$ is the projection perpendicular to it.

Further, we have loop operators constructed from link variables only,

$$
C_{ij}^{1\times1}(x) = \mathrm{Tr}\,\Big(U_i(x)U_j(x+\hat{\imath})U_i^\dagger(x+\hat{\jmath})U_j^\dagger(x)\Big)\,, \quad i,j=1,2,\, i\neq j, \qquad (11)
$$

and in addition to the elementary plaquette $C^{1\times1}$, we also consider squares of size 2×2 as well as rectangles of size 1×2, 1×3, 2×3. Hence, we have five versions of operators consisting of closed loops of gauge fields, *viz.*

$$
C_{ij}^{1\times1},\ C_{ij}^{2\times2},\ C_{ij}^{1\times2},\ C_{ij}^{1\times3},\ C_{ij}^{2\times3}. \qquad (12)
$$

Another pure gauge operator useful to probe the confining properties of the theory is the Polyakov loop along a spatial direction j,

$$
P_j^{(L)}(x) = \mathrm{Tr}\prod_{m=0}^{L-1} U_j(x+m\hat{\jmath}), \quad j=1,2. \qquad (13)
$$

Apart from its relevance for confinement, the Polyakov loop also plays an important rôle in the study of finite size effects. Although single torelons arising from correlations of the Polyakov loop $P_j^{(L)}$ can neither contribute directly to correlations of operators $C^{1\times1},\ldots,C^{2\times3}$, nor to our mixed operators, they may well couple indirectly on the grounds that they share the quantum numbers with the infinite volume states. Furthermore, torelon-antitorelon pairs are known to give rise to finite-volume effects in glueball calculations [18]. Apart from studying correlations of Polyakov loops *per se*, we have thus constructed single-torelon and torelon-pair operators in the 0_+^+ and 2_+^+ channels and studied their correlations as a safeguard against finite-size effects.

2.4 Quantum numbers

Operators with definite quantum number assignments may be constructed from the above operator types by taking linear combinations with appropriate transformation

properties, *i.e.* by applying projection operators for the various irreducible representations of the symmetry group of the lattice slice upon which the operators are constructed.

In a three-dimensional Euclidian gauge theory, the slice is a plane with an $SO(2)$ rotational symmetry and discrete Z_2 parity reflection and charge conjugation symmetries. Rotations are generated by $R(\theta)$ under which operators of angular momentum j gain a phase $\exp[\mathrm{i}j\theta]$. Parity in two spatial dimensions reflects operators in one coordinate axis; $P : (x, y) \to (x, -y)$; reflections in other axes are related to this by rotations. Charge conjugation acts as complex conjugation on the matrix valued fields, $C : U_i(x) \to U_i^*(x), \varphi(x) \to \varphi^*(x)$. Physical states and operators are characterised by their eigenvalues under these operations, the quantum numbers J^{PC}. In contrast to the fundamental Higgs model, there are no $C = -1$ states in the SU(2) pure gauge theory or the SU(2) adjoint Higgs model. In this model SU(2) charge conjugation is equivalent to a global gauge transformation, and hence any gauge-invariant operator is even under this operation. We therefore omit the index C from now on, implying that all states have $C = +1$.

With an adjoint scalar field present, there is an additional Z_2 symmetry corresponding to reflections $\varphi \to -\varphi$, whose eigenvalue we call R. Clearly operators containing an even number of scalar fields, such as A_{ij}^+, will couple to $R = +1$ states, and those with odd, such as A_{ij}^-, to $R = -1$. We thus classify our operators and the states they couple to by J_R^P.

On the lattice the symmetry group is broken from $SO(2) \otimes Z_2(P) \otimes Z_2(R)$ to the point group $C_v^4 \otimes Z_2(R)$, which restricts the allowed rotations to $R(\theta_n)$ where $\theta_n = n\pi/2$. Strictly speaking, we should thus classify our states by the irreducible representations of C_v^4 rather than by J^P. Since we are really interested in continuum physics and, as we shall see, our data reproduce the continuum symmetries within the statistical errors, we prefer to keep the continuum notation.

The fact that the two-dimensional parity operator reflects only one spatial direction, and hence the angular momentum operator changes sign under P, has an important consequence for the spectrum: in $2 + 1$ dimensions all states with $J \neq 0$ come in degenerate pairs of opposite parity (see, *e.g.*, [14]). This statement of "parity doubling" is based on the continuum rotation group, whereas a square lattice with a finite volume only admits rotations in units of $\pi/2$. Thus, although we should continue to observe parity doubling of 1_R^+ and 1_R^- on the lattice, the doubling in the $J = 2$ sector is lost, and will only be recovered in the infinite volume limit. Comparing the masses of the 2_R^+ and 2_R^- states is thus a useful measure of whether our lattice is free from discretisation and finite volume effects. In this study all simulations were done on lattices large enough that parity doubling was, within statistical errors, in accordance with continuum, infinite volume expectations.

An interesting feature of the SU(2) fundamental Higgs model is the near replication of the pure gauge theory glueballs within its spectrum. Whereas one might expect the

excitations of the former to be a mixture of gluonic and scalar degrees of freedom, it is found instead that within the spectrum there are some essentially purely gluonic states. Given their remarkable decoupling from the scalar fields, it is then unsurprising that the masses of these match that of the pure gauge model almost exactly [15]. One of our main interests is to study whether the glueball spectrum survives the addition of adjoint scalar fields similarly unchanged. From the known spectra of the pure gauge theory [14] and of the fundamental representation Higgs model [15] we expect the spin 0 and spin 2 channels to contain the lowest glueball masses, so in order to carry out the necessary mixing analysis, we have constructed large bases of different operator types for these two channels:

0^+_+ channel:

R: $R(x)$
L: $L_1(x) + L_2(x)$
A: $\sum_{n=1}^{4} R(\theta_n) \left(A^+_{12}(x) + P A^+_{12}(x) \right)$
B: $B_\perp(x)$
C: symmetric combinations of $C^{1\times1}$, $C^{2\times2}$, $C^{1\times2}$, $C^{1\times3}$, $C^{2\times3}$
P: $P_1^{(L)}(x) + P_2^{(L)}(x)$
P_d: $P_1^{(L)}(x) \cdot P_2^{(L)}(x)$
T: $\left(P_1^{(L)}(x) \right)^2 + \left(P_2^{(L)}(x) \right)^2$

2^+_+ channel:

R: $R^{(n)}_-(x) \equiv \frac{1}{2} \left\{ \mathrm{Tr}\left[\varphi^{(n,1)}(x) \varphi^{(n,1)}(x) \right] - \mathrm{Tr}\left[\varphi^{(n,2)}(x) \varphi^{(n,2)}(x) \right] \right\}, \quad n > 1$
L: $L_1(x) - L_2(x)$
A: $\sum_{n=1}^{4} \mathrm{e}^{\mathrm{i}n\pi} R(\theta_n) \left(A^+_{12}(x) + P A^+_{12}(x) \right)$
C: antisymmetric combinations of $C^{1\times2}$, $C^{1\times3}$, $C^{2\times3}$
P: $P_1^{(L)}(x) - P_2^{(L)}(x)$
T: $\left(P_1^{(L)}(x) \right)^2 - \left(P_2^{(L)}(x) \right)^2$

In these expressions $R(\theta_n)$ rotates the following brackets by θ_n around x, and P denotes the parity operation. The labels P, P_d refer to single torelon operators, whereas T couples to torelon pairs in the respective channels.

In principle, similarly extended bases are possible for the other channels as well. This requires a lot of memory and computer time, and furthermore the glueballs in the other channels are anticipated to be rather heavy [15, 14], and a mixing analysis would be difficult. The dynamics of mixing is moreover expected to be independent of the precise quantum number channel [15], so it should be sufficient to study the 0^+_+ and 2^+_+ as detailed examples. For the other channels we therefore limit ourselves to just one or

two operator types $B_{||}$ and/or A. We only give two more explicit examples; the other combinations follow straightforwardly.

0^-_- channel:
B: $\sum_{n=1}^{4} R(\theta_n) B_{||}(x)$
A: $\sum_{n=1}^{4} R(\theta_n) \left(A^-_{12}(x) - P A^-_{12}(x) \right)$

1^+_- channel :
B: $\sum_{n=1}^{4} \mathrm{e}^{\mathrm{i}n\pi/2} R(\theta_n) B_{||}(x)$
A: $\sum_{n=1}^{4} \mathrm{e}^{\mathrm{i}n\pi/2} R(\theta_n) \left(A^-_{12}(x) + P A^-_{12}(x) \right)$

For all channels we construct operator versions from elementary as well as blocked fields at various blocking levels. We then take zero momentum sums by averaging over a timeslice, $\phi(t) = 1/L^2 \sum_{x1,x2} \phi(x)$, where $\phi(x)$ denotes a generic operator at some blocking level.

2.5 Matrix correlators

In order to compute the excitation spectra of states with given quantum numbers, we construct matrix correlators by measuring all cross correlations between different types of operators at several blocking levels. The correlation matrix can be diagonalised numerically following a variational method. For a given set of N operators $\{\phi_i\}$ we find the linear combination that minimises the energy, corresponding to the lightest state. The first excitation can be found by applying the same procedure to the subspace $\{\phi_i\}'$ which is orthogonal to the ground state. This may be continued to higher states so that we end up with a set of N eigenstates $\{\Phi_i,\, i = 1, \ldots, N\}$ given by

$$\Phi_i(t) = \sum_{k=1}^{N} a_{ik} \phi_k(t). \tag{14}$$

The coefficients a_{ik} quantify the overlap of each individual operator ϕ_k used in the simulation onto a particular, approximate mass eigenstate Φ_i. For a complete basis of operators this procedure is exact. In practice, the quality of the approximation clearly depends on the number N of original operators and their projection properties. The eigenstates already determined are removed from the basis for the higher excitations, so that the basis for the latter gets smaller and the corresponding higher states are determined less reliably. A more detailed discussion of the calculation and of checks of its stability can be found in [15], where the same procedure was applied to the fundamental Higgs model.

In order to distinguish glueballs and scalar bound states, the most elaborate calculation is done in the 0^+_+ and 2^+_+ channels. For 0^+_+ our basis consists of $N = 32$ operators

$\phi_k \in \{R, L, A, B, C, P, T, P_d\}$, for 2^+_+ we have $N = 31$ and $\phi_k \in \{R, L, A, C, P, T\}$, each operator considered for at least two blocking levels. This typically enables us to extract the four or five lowest lying states in those channels reliably. In the 0^-_-, 2^+_-, 1^+_-, 1^-_- channels we work with $N = 9$ operators $\phi_k \in \{A, B\}$, and in the remaining channels we have $N = 4$ and $\phi_k \in \{A\}$. Correspondingly, in the smaller bases we can only extract the ground state and, in some cases, the first excitation reliably. Finally, in order to compute the string tension we have also diagonalised a separate basis of Polyakov loop operators at $N = 4$ different blocking levels.

2.6 Simulation and analysis

The Monte Carlo simulation of the lattice action, Eq. (4), is performed using the same algorithm as in previous work [7]. The update of gauge variables employs a combination of the standard heatbath and over-relaxation algorithms for SU(2) [19], whereas the scalars are updated by a suitable adaption of the algorithm for fundamental scalars suggested in [20] and employed in [15]. In order to account for the quadratic dependence of the hopping term on the link variables, the link update for the pure gauge action has to be supplemented by a Metropolis step.

We define a "compound" sweep to consist of a combination of one heatbath and several over-relaxation updates of the gauge and scalar fields. In this study we performed 5 over-relaxation steps for every heatbath update. Measurements are taken after every such compound sweep. We have gathered between 5 000 and 30 000 measurements, depending on the lattice sizes which range from 24^3 for the coarsest lattice to 48^3 on the finest one.

All our mass estimates are obtained from measured correlation functions of operators Φ_i in the diagonalised bases defined in the preceding subsection. Correlated fits over some interval $[t_1, t_2]$ are performed to the ansatz for the asymptotic behaviour of the correlation function on a finite lattice, for large T,

$$\langle \Phi_i^\dagger(t)\Phi_i(0)\rangle = A_i \left(\mathrm{e}^{-aM_i\, t} + \mathrm{e}^{-aM_i(T-t)} \right) \ , \tag{15}$$

where i labels the operator, and T denotes the extent of the lattice in the time direction. In cases where the effective masses did not show plateaux long enough to perform a correlated fit, we used the effective masses for our mass estimates.

Statistical errors are estimated using a jackknife procedure for which the individual measurements have been accumulated in bins of $100 - 250$ sweeps.

3 Numerical results

We have performed simulations at temperatures $T = 2T_c$, $T = 4T_c$ and $T = 5T_c$ corresponding to three points $\{x, y\}$ in the metastable confinement phase of the model, as detailed in Table 1.

T	x	y	$\beta = 9$	$\beta = 12$	$\beta = 18$
$2T_c$	0.141	0.185	$L^2 \cdot T = 28^3$, 38^3	$L^2 \cdot T = 38^3$	—
$4T_c$	0.111	0.228	—	$L^2 \cdot T = 38^3$	—
$5T_c$	0.104	0.242	$L^2 \cdot T = 24^3$, 34^3	$L^2 \cdot T = 34^3$	$L^2 \cdot T = 48^3$

Table 1: *The lattice parameters and sizes simulated.*

$T = 2T_c$	$\beta = 9$		$\beta = 12$
	$L = 38$	$L = 28$	$L = 38$
$aM_P(L)$	0.849 (13)	0.627 (6)	0.462 (4)
$a\sqrt{\sigma_\infty}$	0.151 (1)	0.152 (1)	0.112 (1)
$\sqrt{\sigma_\infty}/g_3^2$	0.339 (3)	0.341 (2)	0.336 (2)

Table 2: *Polyakov loop masses and string tensions at $T = 2T_c$.*

The most elaborate test of finite volume effects as well as an explicit continuum extrapolation for the lowest states are done for $T = 5T_c$. Experience of the pure gauge model [14] suggests that to avoid contamination of the spectrum by light torelonic states the lattice size should be $L \geq 24$ at $\beta = 9$. We thus simulate three different lattice spacings (the third one being half of the first) while approximately maintaining this physical volume (*i.e.* $L/\beta = 24/9$, using the lattice spacing as defined by the bare coupling). We find all these couplings to lie in the scaling window of the theory which permits a continuum extrapolation of the low lying masses. To verify that finite volume effects are indeed small we also simulate a second, larger volume at the coarsest lattice spacing.

At $T = 2T_c$ we simulate two lattice spacings and physical volumes, and at $T = 4T_c$ just one as we are by now confident that lattice effects are small. In these cases continuum extrapolation is not possible and we thus use the masses measured at the

$T = 4T_c$	$\beta = 12$
	$L = 38$
$aM_P(L)$	0.476 (4)
$a\sqrt{\sigma_\infty}$	0.114 (1)
$\sqrt{\sigma_\infty}/g_3^2$	0.342 (2)

Table 3: *Polyakov loop masses and string tensions at $T = 4T_c$.*

$T = 5T_c$	$\beta = 9$		$\beta = 12$	$\beta = 18$
	$L = 34$	$L = 24$	$L = 34$	$L = 48$
$aM_P(L)$	0.80 (1)	0.554 (5)	0.426 (4)	0.257 (6)
$a\sqrt{\sigma_\infty}$	0.155 (1)	0.155 (1)	0.114 (1)	0.075 (1)
$\sqrt{\sigma_\infty}/g_3^2$	0.349 (2)	0.349 (2)	0.342 (3)	0.338 (4)

Table 4: *Polyakov loop masses and string tension at* $T = 5T_c$.

smallest lattice spacing as approximations of the continuum result.

In order to perform continuum extrapolations it is necessary to have some definition of the lattice spacing with which to scale the dimensionless lattice masses. The simplest measure comes from the bare gauge coupling, $a = 4/(\beta g_3^2)$. Such a formula is liable to quantum corrections, which in some cases translate as large $\mathcal{O}(a)$ corrections to the naïve scaling of the masses [21]. A non-perturbative definition of the lattice spacing should in principle avoid this, and in pure gauge theory it is customary to scale all lattice masses in units of the string tension. We thus discuss this quantity first.

3.1 The string tension

As explained previously, a Polyakov loop in a spatial plane couples to a flux loop state (or torelon) that winds around the periodic boundaries of the finite volume. The exponential fall–off of its correlator is related to the mass of the flux loop, according to

$$\sum_{\mathbf{x}} \left\langle P_j^{(L)}(x) P_j^{(L)\dagger}(0) \right\rangle \simeq e^{-aM_P(L)t}, \quad aM_P(L) = a^2\sigma_L L. \tag{16}$$

Such a flux loop state can be easily identified through its energy scaling linearly with the size of the lattice, as seen in the entries labelled by P in Tables 5, 7 and 9. In contrast to the fundamental Higgs model, there are no fundamental representation matter fields in the action to screen the colour flux of static charges leading to a breaking of flux tubes longer than a screening length [22]. On the contrary, a flux tube between fundamental charges will persist to infinite separation as in the pure gauge theory, and a string tension can be defined in precisely the same way by the slope of the static potential at infinite separation[1]. Accordingly, periodic flux loops winding through the boundaries of the lattice will not be screened, and the coefficient σ_L corresponds to the string tension on a finite volume. An estimate for the string tension in infinite volume is then provided by the relation [23]

$$a^2\sigma_\infty = a^2\sigma_L + \frac{\pi}{6L^2}. \tag{17}$$

[1] To avoid confusion, we note that this is the string tension in the $2+1$ dimensional theory, corresponding to the *spatial* string tension in the $3+1$ dimensional theory at finite temperature.

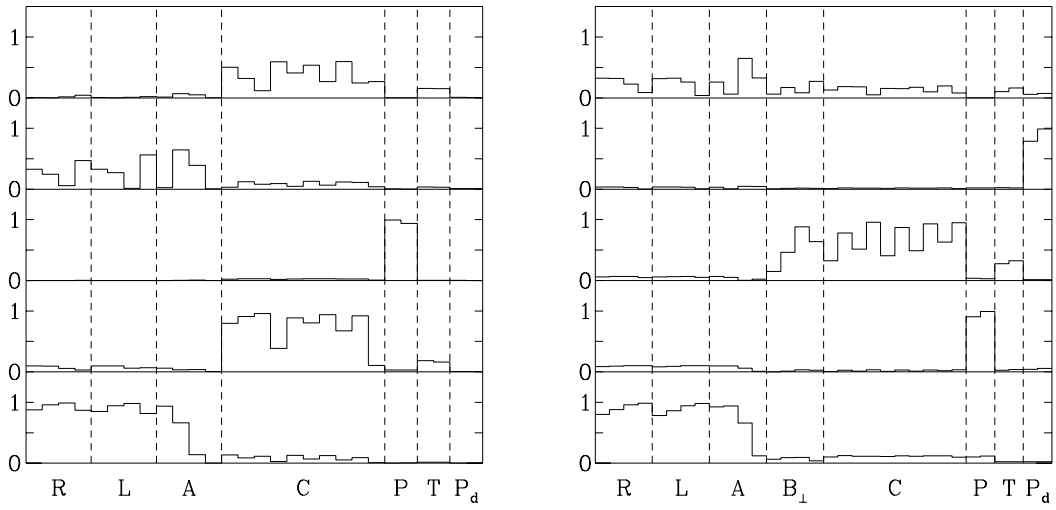

Figure 1: *The coefficients a_{ik} of the operators used in the simulation for the five lowest 0^+_+ eigenstates for 28 operators at $\beta = 9$ (left), and for 32 operators at $\beta = 18$ (right).*

We have diagonalised a basis of Polyakov loop operators and the results are summarised in Tables 2–4. As we shall see with the glueball masses, the string tension is barely affected by the presence of the scalar fields. It also shows little dependence on the scalar parameters x, y.

Expressing the string tension in units of the bare coupling, we may (linearly) extrapolate the results at $T = 5T_c$ to the continuum, where we find $\sqrt{\sigma_\infty}/g_3^2 = 0.326(7)$, which compares to $\sqrt{\sigma_\infty}/g_3^2 = 0.3353(18)$ in pure gauge theory [14]. That the slope of this extrapolation is small indicates that the difference between using a tree level definition of the lattice spacing, and a non–perturbative one is slight, and in most cases any improvements in using the string tension as opposed to the bare coupling for setting the scale are outweighed by the additional statistical errors on the former.

For this reason, in the following tables we scale and quote masses in units of the bare continuum coupling to allow rapid comparisons of measurements at different β.

3.2 The mass spectrum

A detailed account of the mass estimates for the lowest states computed on the various lattices is given in Tables 5–10, together with the dominant operator content of a given mass eigenstate for the channels with the largest operator bases.

Let us discuss in detail only the $T = 5T_c$ parameter set, the procedure being entirely analogous for the others. As an example for the identification of the operator

$T = 2T_c$	$\beta = 9$				$\beta = 12$	
state	$L^2 \cdot T = 38^3$		$L^2 \cdot T = 28^3$		$L^2 \cdot T = 38^3$	
0^+_+	M/g_3^2	Ops.	M/g_3^2	Ops.	M/g_3^2	Ops.
Φ_1	0.747 (7)	R, L, A	0.743 (7)	R, L, A	0.744 (9)	R, L, A
Φ_2	1.629 (27)	$C, B_\perp$	1.411 (18)	P	1.416 (15)	P
Φ_3	2.007 (45)	$A, (R, L)$	1.613 (23)	$C, B_\perp$	1.623 (21)	$C, B_\perp$
Φ_4	1.913 (45)	P	1.980 (36)	$A, (R, L)$	1.998 (27)	$A, (R, L)$
Φ_5	2.22 (6)	$C, B_\perp$	2.36 (6)	$C, B_\perp$	2.34 (4)	$C, (B_\perp)$
Φ_6	2.80 (13)	A	2.47 (9)	P_d	2.38 (5)	P_d
Φ_7	2.94(17)	$C, (B_\perp)$	2.75 (11)	A	2.79 (7)	$C, B_\perp$
Φ_8	3.11 (48)	(P)	2.86 (13)	$C, B_\perp$	2.83 (7)	(A)
2^+_+	M/g_3^2	Ops.	M/g_3^2	Ops.	M/g_3^2	Ops.
Φ_1	1.94 (5)	P	1.440 (22)	P	1.401 (15)	P
Φ_2	1.92 (5)	P	1.454 (18)	P	1.419 (18)	P
Φ_3	2.27 (6)	R, L, A	2.24 (5)	R, L, A	2.30 (4)	R, L, A
Φ_4	2.61 (11)	C	2.34 (8)	(P)	2.37 (5)	(P)
Φ_5	2.60 (29)	(P)	2.70 (12)	C	2.65 (5)	C
Φ_6	3.15 (19)	C	3.05 (15)	C, T	2.98 (8)	C, T

Table 5: *Mass estimates and dominant operator contributions in the 0^+_+ and 2^+_+ channels at $T = 2T_c$. The dominant operator types contributing are denoted with (without) parentheses if $a_{ik} < (>) 0.5$.*

content of a mass eigenstate, we display the coefficients a_{ik} (*cf.* Eq. (4)) of the five lowest mass eigenstates in the 0^+_+-channel in Fig. 1 for our largest and smallest lattice spacing. The operator contributions listed in Table 9 are those which have coefficients a_{ik} larger than 0.5. If the state has weak overlap with all operators of our basis and the dominant coefficients are smaller than 0.5, we indicate this by parentheses in the table. The ordering of states Φ_i was obtained during the diagonalisation procedure from the effective mass of the corresponding correlator on the first timeslice.

As in the confinement phase of the fundamental representation Higgs model [15], we find here a dense spectrum of bound states also. In [15] it was found that the Yang-Mills glueball spectrum is repeated almost identically in the model with fundamental scalar fields, with additional bound states of scalars, and little mixing between them. An interesting question is whether the situation is similar in the case with adjoint scalar fields. Fig. 1 (left) shows that this is indeed so. The ground state is clearly dominated by scalar operators, whereas the first as well as the fourth excited state have almost exclusively gluonic contributions and hence are identified as glueballs. Fig. 1 (right) is the same for our finest lattice, but now with four blocked versions

$T = 2T_c$	$\beta = 9$		$\beta = 12$
state	$L = 38$	$L = 28$	$L = 38$
0^-_+	—	—	3.24 (12)
0^-_-	1.229 (14)	1.220 (14)	1.118 (12)
0^{-*}_-	2.14 (6)	2.14 (6)	2.16 (4)
1^+_+	—	—	3.04 (12)
1^-_+	3.00 (5)	3.01 (5)	2.93 (11)
1^+_-	2.02 (2)	2.01 (2)	1.99 (3)
1^-_-	1.95 (5)	1.87 (8)	1.92 (5)
2^+_-	2.41 (9)	2.57 (9)	2.52 (6)
2^-_+	2.35 (3)	2.36 (6)	2.31 (5)

Table 6: *Masses M/g_3^2 for the other channels at $T = 2T_c$.*

$T = 4T_c$	$\beta = 12$	
state	$L^2 \cdot T = 38^3$	
0^+_+	M/g_3^2	Ops.
Φ_1	0.945 (9)	R, L, A
Φ_2	1.425 (15)	P
Φ_3	1.626 (18)	$C, B_\perp$
Φ_4	2.151 (30)	$A, (R, L)$
Φ_5	2.33 (4)	$C, B_\perp$
Φ_6	2.33 (4)	(P)
Φ_7	2.43 (5)	P_d
Φ_8	2.84 (7)	C
2^+_+	M/g_3^2	Ops.
Φ_1	1.428 (21)	P
Φ_2	1.452 (18)	P
Φ_3	2.42 (4)	R, L, A
Φ_4	2.34 (5)	(P)
Φ_5	2.63 (6)	C
Φ_6	3.02 (8)	C, T

Table 7: *Mass estimates and dominant operator contributions in the 0^+_+ and 2^+_+ channels at $T = 4T_c$. The dominant operator types contributing are denoted with (without) parentheses if $a_{ik} < (>)0.5$*

$T = 4T_c$	$\beta = 12$
state	$L = 38$
0^-_+	3.48 (12)
0^-_-	1.323 (12)
0^{-*}_-	2.30 (4)
1^+_+	3.47 (24)
1^-_+	3.05 (11)
1^+_-	2.00 (3)
1^-_-	2.05 (4)
2^+_-	2.57 (5)
2^-_+	2.45 (5)

Table 8: *Masses M/g_3^2 for the other channels at $T = 4T_c$.*

of the operator $B_\perp$ (*cf.* Eq. (10)) included in addition to the operators used for the left plot. At first sight this appears to violate the "non-mixing" between scalar and gluonic states as observed with the smaller basis. Upon expanding and taking the trace in Eq. (10), however, one readily sees that the operator is in fact a sum of terms of the form $B_\perp \sim \mathrm{Tr}\,(U^2) + B_{||}^2 + \mathrm{Tr}\,(\varphi^2)B_{||}^2$. Of these, the first term mixes with our other loop operators and has projection onto the glueball states since ($\mathrm{Tr}\,(U^2)$ has the same representation content as $\mathrm{Tr}\,(U)$), whereas the other terms project onto higher excitations (they are of higher dimension) and thus die out asymptotically. Hence, the operator $B_\perp$ asymptotically behaves as a C-type operator which mainly projects onto glueballs, but very little onto scalar states, as is corroborated in Fig. 1. This figure further shows that the decoupling of the gluonic sector is stable under variations of the lattice spacing by a factor of two. As we shall see, with the lattice spacings considered we are quite close to the continuum, and the observed effect should persist in the continuum limit. This picture is repeated in the 2^+_+ channel.

The spectrum of higher excitations becomes increasingly dense with increasing energy. For the 0^+_+ and 2^+_+ channels, the eigenstates beyond Φ_6 become increasingly difficult to identify, and their total overlap with the operators in the basis becomes smaller. Further, they are closer in energy and within our statistical errors appear often degenerate. An unambiguous resolution of these states would require still larger bases as well as more statistics. We have therefore chosen not to quote them as reliable results.

Another word of caution concerns the states 0^-_+, 1^+_+ and 1^-_+. As described in Sec. 2.5, the bases for these states consist exclusively of four blocked versions of the operator type A. It is conceivable that these operator sets have very poor projection onto some of the sought ground states, leading to an overestimate of their masses. Indeed, such

$T = 5T_c$	$\beta = 9$			
state	$L^2 \cdot T = 34^3$		$L^2 \cdot T = 24^3$	
0^+_+	M/g_3^2	Ops.	M/g_3^2	Ops.
Φ_1	1.010 (9)	R, L, A	1.010 (12)	R, L, A
Φ_2	1.61 (5)	C	1.24 (3)	P
Φ_3	1.82 (7)	P	1.64 (3)	$C, B_\perp$
Φ_4	2.19 (14)	L, A	2.16 (11)	L, A
Φ_5	2.29 (16)	C	2.05 (13)	P_d
Φ_6	2.73 (15)	(P)	2.36 (18)	$C, B_\perp$
2^+_+	M/g_3^2	Ops.	M/g_3^2	Ops.
Φ_1	1.795 (32)	P	1.215 (25)	P
Φ_2	1.798 (32)	P	1.253 (25)	P
Φ_3	2.35 (8)	R, L, A	2.25 (10)	(P)
Φ_4	2.68 (11)	C	2.45 (15)	R, L, A
Φ_5	2.67 (11)	(P)	2.57 (11)	C, T
Φ_6	2.87 (18)	C	2.86 (11)	C, T
Φ_7	3.34 (24)	R, L, A	3.17 (17)	R, L, A

$T = 5T_c$	$\beta = 12$		$\beta = 18$	
state	$L^2 \cdot T = 34^3$		$L^2 \cdot T = 48^3$	
0^+_+	M/g_3^2	Ops.	M/g_3^2	Ops.
Φ_1	1.005 (12)	R, L, A	1.008 (18)	R, L, A
Φ_2	1.26 (3)	P	1.152 (27)	P
Φ_3	1.63 (3)	$C, B_\perp$	1.60 (5)	$C, B_\perp$
Φ_4	2.19 (8)	A	1.91 (5)	P_d
Φ_5	2.33 (8)	$C, B_\perp, (T)$	2.19 (7)	A
Φ_6	2.25 (8)	P_d	2.29 (9)	C, T
2^+_+	M/g_3^2	Ops.	M/g_3^2	Ops.
Φ_1	1.266 (21)	P	1.143 (27)	P
Φ_2	1.274 (24)	P	1.161 (27)	P
Φ_3	2.32 (4)	(P)	2.38 (5)	(P)
Φ_4	2.43 (5)	R, L, A	2.51 (7)	C, T
Φ_5	2.61 (5)	$C, (T)$	2.45 (8)	L, A
Φ_6	2.78 (6)	C, T	2.72 (6)	C
Φ_7	3.23 (11)	L	3.17 (10)	A

Table 9: *Mass estimates and dominant operator contributions in the 0^+_+ and 2^+_+ channels at $T = 5T_c$. The dominant operator types contributing are denoted with (without) parentheses if $a_{ik} < (>)0.5$.*

$T = 5T_c$	$\beta = 9$		$\beta = 12$	$\beta = 18$
state	$L^2 \cdot T = 34^3$	$L^2 \cdot T = 24^3$	$L^2 \cdot T = 34^3$	$L^2 \cdot T = 48^3$
0^-_+	—	—	3.39 (15)	—
0^-_-	1.352 (27)	1.368 (28)	1.342 (33)	1.340 (30)
0^{-*}_-	2.34 (8)	2.28 (6)	2.33 (8)	2.28 (5)
1^+_+	3.01 (37)	3.65 (37)	3.52 (37)	—
1^-_+	3.02 (26)	3.16 (20)	3.20 (20)	—
1^+_-	2.13 (3)	2.04 (5)	2.06 (6)	—
1^-_-	2.02 (6)	2.09 (5)	2.06 (5)	—
2^+_-	2.69 (4)	2.60 (10)	2.64 (9)	—
2^-_+	2.52 (10)	2.60 (9)	2.54 (10)	—

Table 10: *Masses M/g_3^2 for the other channels at $T = 5T_c$.*

an effect was encountered in the 1^P_- sectors, as is apparent from comparing the two different parity states, which should be degenerate. This problem can only be solved with a larger basis including other operator types. For 2^-_+ the basis equally consists of four operators of type A. In this case, however, we observe parity doubling with the ground state in the 2^+_+ channel (see below), and may thus be confident to have good projection on the 2^-_+ ground state.

At our largest lattice spacing, $\beta = 9$, we have performed an explicit check for finite volume effects. Comparison of the corresponding columns in Table 9 shows that the masses for those states that do not couple to winding operators (P, P_d, T) are statistically compatible on $L^2 \cdot T = 24^3$ and $L^2 \cdot T = 34^3$. It appears that already on the smaller volume most of our results for the spectrum are free of finite size effects, as was the case in the pure gauge theory. Of the operator eigenvectors projecting onto winding operators, those purely of type P or P_d may be discounted as mere finite volume artefacts, they disappear from the spectrum in the infinite volume limit. More difficult are those states that couple both to non-winding, C or $B_\perp$, and to winding operators, T, such as the 2^+_+ states Φ_5 and Φ_6 whose masses are likely to suffer most from finite volume effects. At $\beta = 9$, where we have two volumes, we can resort to the larger lattice where the states are decoupled from the torelons, and trust that this number is as close to the infinite volume limit as the other states. On the finer lattices, however, we have only one volume, and hence it is likely that the corresponding masses are affected by the admixture of torelons to these states.

As we have discussed, one important signal of finite volume and discretisation effects is the loss of parity doubling in the spectrum. On all our lattices we find within statistical errors a degeneracy of the J^+_R and J^-_R states not only for $J = 1$ (where it is expected even on the lattice) but also for $J = 2$. In the latter case, the relevant

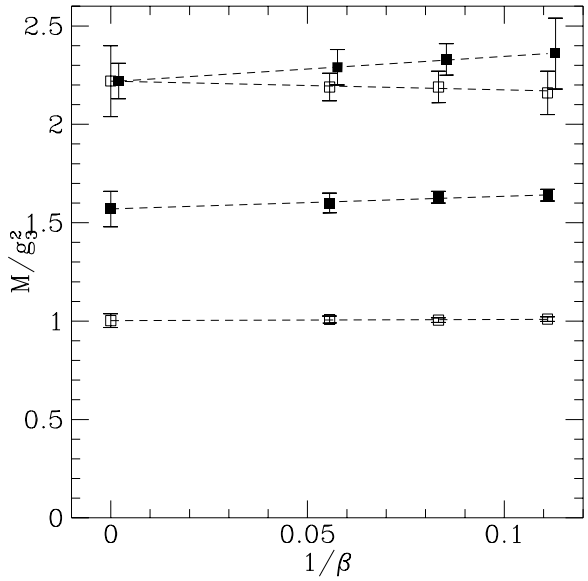

Figure 2: *The approach to the continuum of the four lowest* 0_+^+ *states at* $T = 5T_c$. *Filled symbols denote glueballs, open symbols bound states of scalars.*

comparison is between non–torelonic states that do not couple to winding operators (and thus remain of finite mass in the infinite volume extrapolation).

We have already commented that in extrapolating to the continuum limit there is a choice in the method of defining the lattice spacing. There is also some freedom in the functional form of the extrapolation. From the weak coupling expansion of the lattice action, the lowest order corrections to the continuum limit mass should be linear in the lattice spacing. Thus if we are sufficiently close to the continuum limit, a straight line fit to the data can be attempted.

We have performed linear fits for the low lying 0_+^+ and 2_+^+ states, using both tree level and non-perturbative definitions of the lattice spacing. All fits give acceptable $\chi^2/\text{d.o.f.} < 1$. In Fig. 2 we show such fits using units of the bare coupling, and it is such a fit that we use for the ground state in the 2_+^+ channel. Given the very large errors on the gradient for linear fits using the string tension to set the scale, we have insufficient data to decide if the latter, non-perturbative definition of the lattice spacing improves the scaling behaviour.

The results for 0_+^+ and 2_+^+ are given in Table 11. The 2_+^+ pure glueball couples to torelons on our finest lattice, so that its mass value there could not be used for an extrapolation. We quoted the value for $\beta = 12$ instead. We also compare with the corresponding glueball states in the pure gauge theory and find their masses to deviate at the percent level at most from those measured in the Higgs model. We conclude that

0^+_+ channel			2^+_+ channel		
gauge-Higgs		pure gauge	gauge-Higgs		pure gauge
scalar	glueball	glueball	scalar	glueball	glueball
1.002 (35)			2.46 (21)		
	1.57 (9)	1.58 (1)		2.61 (5)	2.62 (5)
2.22 (18)					
	2.22 (25)	2.29 (3)			

Table 11: *Final mass estimates using the continuum extrapolation in the bare coupling of our data at $T = 5T_c$. Our data for the glueball are compared with the results obtained in the pure gauge theory [14].*

we have a situation analogous to the fundamental Higgs model, with the pure gauge glueball spectrum being repeated, with additional bound states of adjoint scalars and little mixing between them.

As comparison of Tables 11 and 9 elucidates, the difference between the masses extrapolated to the continuum and those computed at finite lattice spacing are very small, of the order of a few percent for the lowest states, and mostly covered by the statistical errors of the values on the finest lattice. We therefore quote the latter for the other channels as well as our other parameter sets, noting, however, that for the heavier states this may well amount to an estimated 5% systematic error.

4 Discussion

With the numerical results for various correlation functions at hand, let us now discuss their implications for the spectrum of static correlation functions in four-dimensional SU(2) Yang-Mills theory at finite temperature. In order to express the masses entirely in units of temperature, we have to make use of the perturbative expression for the gauge coupling at that temperature scale, Eq. (3). Using this expression we have $g_3^2(2T_c) \approx 3.83T$, $g_3^2(2T_c) \approx 3.07T$ and $g_3^2(5T_c) \approx 2.89T$. The spectrum in these units is shown in Fig. 3.

4.1 Comparison with four dimensions

The first important question concerns the comparison with a four-dimensional simulation, in order to assess the quality of dimensional reduction in the temperature range under study. A detailed analysis of the low lying modes for SU(2) gauge theory has recently been presented [9] for the temperature range $2T_c < T < 4T_c$. Only the ground states in each quantum number channel are so far available in four dimensions, however.

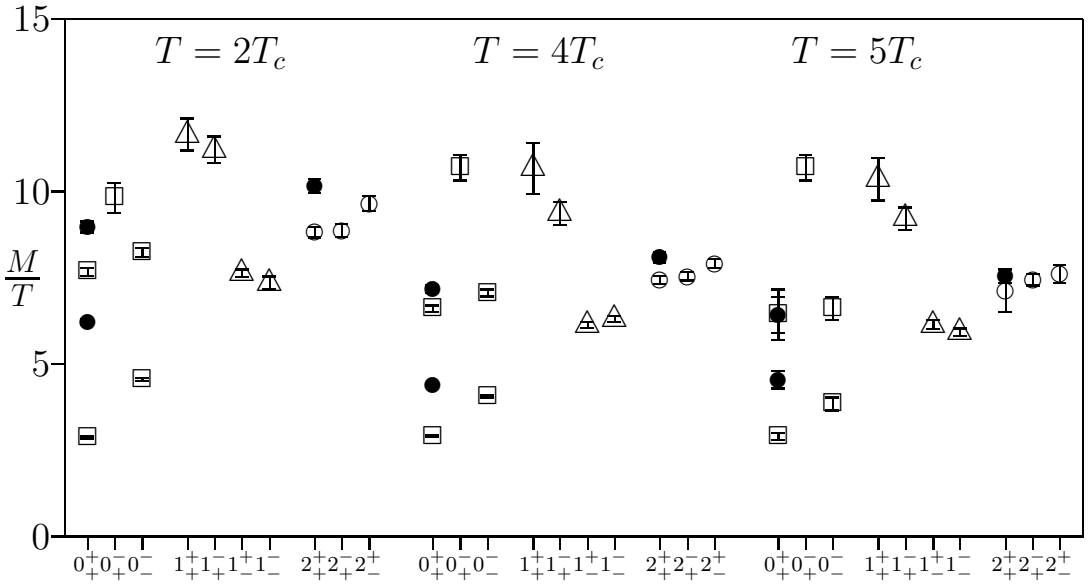

Figure 3: *The spectrum of the lowest inverse static correlation lengths at each temperature. Filled symbols denote glueballs, open symbols bound states of scalars.*

To facilitate the comparison we briefly summarise the situation in four dimensions. There the lattice symmetry group is $D_{4h} \otimes Z(2)_{R_{\tilde{z}}}$ where D_{4h} is the point group of the discretised $2+1$ dimensional space-time slice used to create screening state operators, and $R_{\tilde{z}}$ is the Euclidian time reversal operator in the notation of [24]. It acts on the time component of the gauge field as $R_{\tilde{z}} A_0^a \to -A_0^a$. Dimensional reduction converts the A_0 component of the gauge field into an adjoint scalar field, and the scalar reflection symmetry is the "daughter" of Euclidian time reflection in the original theory.

As the temperature is increased in the four-dimensional theory, the timelike direction of the slice becomes squeezed, to the point where the slice becomes quasi–two-dimensional, and the effective symmetry group becomes C_v^4. At this point the spectrum of screening masses should conform to a pattern predicted by this latter symmetry group, as has indeed been observed [9]. If the perturbative matching of finite temperature SU(2) pure gauge theory to the SU(2) adjoint Higgs model in three dimensions is correct, the screening masses should furthermore match those observed in this study. Hence we expect to see the $3+1$ dimensional D_{4h} states A_1^+ and A_2^- converging on the 0^+ mass we measure (the quantum numbers $R_{\tilde{z}}$, R are suppressed here), and the A_1^- and A_2^+ on the 0^-. The E states should agree with the $J = 1$. The B_1^+ and B_2^- should agree with the 2^+, and B_1^- and B_2^+ should have a common mass with the 2^-. For a more detailed account of this symmetry breaking pattern we refer to [9].

In [9, 10] and the above paragraph discussing the mapping of states, the behaviour under Euclidian time reflection $R_{\tilde{z}}$ has not been specified. This leaves room for potential

ambiguities in comparing the states. For our comparison, we assume that the lowest states have been extracted in [9], without explicit specification of their $R_{\bar{z}}$-symmetry. Correspondingly, for the same spin and parity we compare with the lighter of our R-states. Further, because of parity doubling, B_1^- has to be degenerate with B_1^+ in the continuum limit. In [10], B_1^+ still exhibits finite size effects, so that we take B_1^- instead to compare with our 2_+^+ state. The four-dimensional data are taken from Table 4 in [9] and Table 2 in [10].

The comparison of screening masses after these identifications is shown in Fig. 4. Comparing the temperature dependence of the screening masses, we find agreement for the qualitative behaviour of the lowest states in all channels. Their temperature dependence is weak, with the 0_+^+ slightly rising whereas all other ground states drop with T. In our simulation we find in addition that the temperature dependence becomes stronger for the higher excitations, *cf.* Fig. 3. But even on a quantitative level, we find a remarkable agreement for the low lying states. This could not have been anticipated given that the temperature is rather close to the phase transition, where we know the effective theory description has to break down. The only notable disagreement between the measurement in the full and the reduced theory is for the lightest spin 2 screening mass. But in comparing the heavier screening masses we have to remind ourselves that the effective theory is obtained by integrating out the non-zero Matsubara modes, whose smallest is of the order of $\sim 2\pi T$. The lowest spin 2 screening mass, on the other hand, is already larger than $\sim 6T$ for the temperatures considered, and hence belongs to an energy region where the effective theory loses its validity. In this régime the non-local terms and terms of higher dimension which have been discarded in the construction of the effective theory [5] are no longer suppressed, and disagreement for screening masses of that order and higher is in fact expected.

We conclude that the three-dimensional SU(2) adjoint Higgs model in its metastable symmetric phase is the correct effective theory to describe the static correlation functions in a four-dimensional SU(2) pure gauge theory at finite temperature. The effective theory gives the correct qualitative picture, and for the screening masses in the expected range of validity of the effective theory even quantitative results at temperatures as low as $T = 2T_c$.

4.2 The Debye mass

Of particular interest for non-Abelian plasma physics is the Debye screening mass, which may be expanded as

$$m_D = m_D^{LO} + \frac{N g_3^2}{4\pi} \ln \frac{m_3}{g_3^2} + c_N g_3^2 + \mathcal{O}(g^3 T). \tag{18}$$

The leading order result is known perturbatively [25] to be

$$m_D^{LO} = m_3 = \left(\frac{N}{3} + \frac{N_f}{6} \right)^{1/2} gT. \tag{19}$$

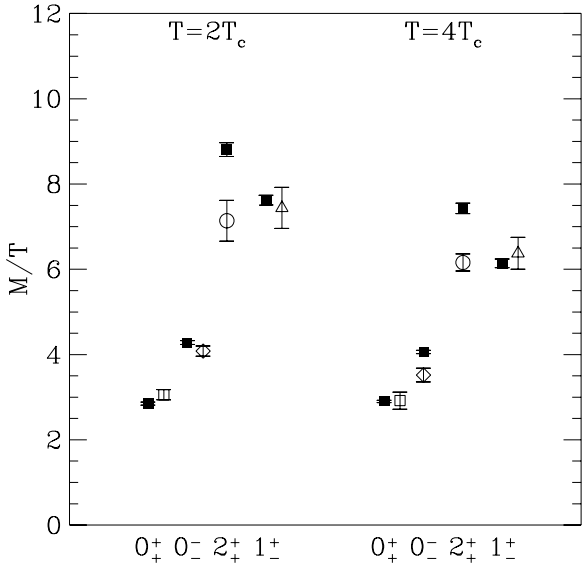

Figure 4: *Comparison of screening masses as calculated in four dimensions directly [9] (open symbols) and from the reduced three-dimensional theory used here (full symbols). In the point group notation of [9], the open squares denote* A_1^+*, diamonds* A_1^-*, circles* B_1^- *and triangles* E^+*.*

	m_D/g_3^2	$(1+2)/g_3^2$	c_2	$\mathcal{O}(g^3T)/g_3^2$
$T = 2T_c$	1.12 (2)	0.296	1.14(4)	-0.32(6)
$T = 4T_c$	1.32 (2)	0.360	1.14(4)	-0.18(6)
$T = 5T_c$	1.34 (3)	0.379	1.14(4)	-0.18(7)

Table 12: *The different contributions to the Debye mass, Eq. (18), where (1+2) is the sum of the first two terms.*

At next-to leading order $\sim g^2T$, one can extract perturbatively a logarithm [26], but c_N is entirely non-perturbative and has to be evaluated by lattice simulations. A gauge invariant, non-perturbative definition for m_D has been given in [24] and is based on Euclidian time reflection, $R_{\tilde{z}}$. According to the definition in [24], the Debye mass m_D corresponds to the mass of the lightest state odd under this transformation, *i.e.* the lightest $R = -1$ state. According to our measurements this is the 0^- ground state, as obtained from the operator $B_{||}$. As discussed in the previous section, our measurement is entirely consistent with the four-dimensional one, see Fig. 4.

On the other hand, c_2 has been determined directly in recent simulations [27, 28] after integrating out A_0 following a prescription in [24]. There the value $c_2 = 1.14(4)$ was found for the leading correction to the perturbative result[2].

Taking these data together, we are now in a position to assess the size of the various contributions in the expansion Eq. (18). These are summarised in Table 12.

The emerging picture is quite interesting: the Debye mass is entirely non-perturbative, with its leading order value being much smaller than the g^2T correction up to temperatures of the order of $T \sim 10^7 T_c$ [28]. On the other hand, the $\mathcal{O}(g^3T)$ corrections are only 20% at temperatures as low as $T = 2T_c$, decreasing rapidly to 10% at $T = 5T_c$.

We thus have to conclude that the scale dominating the physics of electric screening is the scale of the three-dimensional effective theory g_3^2, or equivalently, the soft modes $\sim g^2T$ of the original finite temperature theory, contrary to the naïve expectation $\sim gT$. The contributions on this scale are entirely non-perturbative. Contributions of higher powers in g, on the other hand, can be viewed as small perturbations.

[2]We remark that the operator $B_{||}$ has been simulated previously to determine the Debye mass [29]. By fitting Eq. (18) to the temperature dependence of the mass of $B_{||}$, these authors find the term $\mathcal{O}(g^3T)$ to be consistent with zero, and upon subtracting the perturbative piece m_D^{LO} determine the next-to-leading order correction to be $c_2 = 1.58(20)$. We consider this likely to be an overestimate, as it is two standard deviations above the results of [27, 28]. Adding the perturbative contribution and no other corrections, the resulting m_D likewise deviates from the four-dimensional result of [9] and our present measurements.

5 Conclusions

We have performed a detailed simulation of the spectrum of the SU(2) adjoint Higgs model in $2+1$ dimensions at various points in its metastable confinement phase. The choice of the parameter values was motivated by the connection with four-dimensional SU(2) pure gauge theory at finite temperature, for which the adjoint Higgs model emerges as an effective theory for the static modes after perturbative dimensional reduction. Our results are relevant both for the study of confinement in three-dimensional gauge theories, as well as for the question whether dimensional reduction is applicable to SU(2) pure gauge theory, and eventually to QCD.

Regarding three-dimensional gauge theories, we found a dense spectrum of bound states, which consists of an almost unchanged replica of the glueball spectrum of pure gauge theory, to which additional bound states of adjoint scalars are added. The glueball and scalar states show very little mixing, and correspondingly the string tension is very close to its pure gauge value. The pure gauge quantities are furthermore insensitive to variations of the scalar parameters in the action. All these findings are completely analogous to the situation in the SU(2) fundamental Higgs model [15]. We conclude that the approximate decoupling of the pure gauge sector from the scalar sector is a very robust phenomenon in three dimensions, for which an explanation is lacking at present.

Regarding its rôle as effective theory, we find that dimensional reduction works remarkably well down to temperatures of $2T_c$, where the lowest screening masses computed in the effective and the full theories agree quantitatively. This agreement is rather striking for a temperature so close to the transition. These findings confirm the SU(2) adjoint Higgs model as the correct effective high temperature theory to describe the thermodynamics of four-dimensional SU(2) pure gauge theory. In particular, our investigation has established unambiguously that the A_0 degrees of freedom for temperatures not too far above the phase transition constitute the lightest state in the three-dimensional effective theory, and hence may not be integrated out, as already discussed in [5, 28]. It furthermore implies that the naïve hierarchy of scales $gT \ll g^2T$ does not translate into a corresponding separation of the dynamics of the A_0 and A_i in this temperature range.

We expect no qualitative changes when moving from SU(2) to SU(3). An analogous investigation for SU(3) and three flavours of quarks poses no additional complications and appears desirable in the light of our results.

Acknowledgments

We thank UKQCD for computer time on one of their workstations in Edinburgh where part of these computations were performed, and M. Laine for a critical reading of the manuscript. This work was supported in part by United Kingdom PPARC grant GR/L22744.

References

[1] P. Ginsparg, Nucl. Phys. B 170 (1980) 388;
T. Appelquist and R. Pisarski, Phys. Rev. D 23 (1981) 2305.

[2] K. Kajantie, M. Laine, K. Rummukainen and M. Shaposhnikov, Phys. Rev. Lett. 77 (1996) 2887 [hep-ph/9605028];
M. Gürtler, E.-M. Ilgenfritz and A. Schiller, Phys. Rev. D 56 (1997) 3888 [hep-lat/9704013];
F. Karsch, T. Neuhaus, A. Patkós and J. Rank, Nucl. Phys. Proc. Suppl. 53 (1997) 623 [hep-lat/9608087].

[3] W. Buchmüller and O. Philipsen, Nucl. Phys. B 443 (1995) 47; Phys. Lett. B 397 (1997) 112 [hep-ph/9612286];
N. Tetradis, Nucl. Phys. B 488 (1997) 92 [hep-ph/9608272].

[4] F. Csikor, Z. Fodor, J. Heitger, Phys. Rev. Lett. 82 (1999) 21 [hep-ph/9809291];
M. Laine, JHEP 9906 (1999) 020 [hep-ph/9903513].

[5] K. Kajantie, M. Laine, K. Rummukainen and M. Shaposhnikov, Nucl. Phys. B 503 (1997) 357 [hep-ph/9704416].

[6] E. Braaten and A. Nieto, Phys. Rev. Lett. 76 (1996) 1417; Phys. Rev. D 53 (1996) 3421 [hep-ph/9510408].

[7] A. Hart, O. Philipsen, M. Teper and J. Stack, Phys. Lett. B 396 (1997) 217 [hep-lat/9612021].

[8] J. Fingberg, U. Heller and F. Karsch, Nucl. Phys. B 392 (1993) 493 [hep-lat/9208012].

[9] S. Datta and S. Gupta, Nucl. Phys. B 534 (1998) 392 [hep-lat/9806034].

[10] S. Datta and S. Gupta, [hep-lat/9906023].

[11] P. Lacock, D. Miller and T. Reisz, Nucl. Phys. B 369 (1992) 501.

[12] F. Karsch, M. Oevers and P. Petreczky, Phys. Lett. B 442 (1998) 291;
U. Heller, F. Karsch and J. Rank, Phys. Rev. D 57 (1998) 1438.

[13] P. Lacock, D.E. Miller, B. Petersson and T. Reisz, Nucl. Phys. B 418 (1994) 3 [hep-lat/9310014].

[14] M. Teper, Phys. Rev. D 59 (1999) 014512 [hep-lat/9804008].

[15] O. Philipsen, M. Teper and H. Wittig, Nucl. Phys. B 469 (1996) 445 [hep-lat/9602006];
Nucl. Phys. B 528 (1998) 379 [hep-lat/9709145]

[16] M. Laine, Nucl. Phys. B 451 (1995) 484 [hep-lat/9504001].

[17] M. Teper, Phys. Lett. B 187 (1987) 345.

[18] C. Michael, J. Phys. G 13 (1987) 1001.

[19] K. Fabricius and O. Haan, Phys. Lett. B 143 (1984) 459;
A.D. Kennedy and B.J. Pendleton, Phys. Lett. B 156 (1985) 393.

[20] B. Bunk, Nucl. Phys. B (Proc. Suppl.) 42 (1995) 566.

[21] G. D. Moore, Nucl. Phys. B 523 (1998) 569 [hep-lat/9709053].

[22] O. Philipsen and H. Wittig, Phys. Rev. Lett. 81 (1998) 4056 [hep-lat/9807020].

[23] P. de Forcrand, G. Schierholz, H. Schneider and M. Teper, Phys. Lett. 160 B (1985) 137.

[24] P. Arnold and L. Yaffe, Phys. Rev. D 52 (1995) 7208 [hep-ph/9508280].

[25] E. Shuryak, Zh. Eksp. Teor. Fiz. 74 (1978) 408 [Sov. Phys. JETP 47 (1978) 212];
J. Kapusta, Nucl. Phys. B 148 (1979) 461;
D. Gross, R. Pisarski and L. Yaffe, Rev. Mod. Phys. 53 (1981) 43.

[26] A.K. Rebhan, Phys. Rev. D 48 (1993) R3967 [hep-ph/9308232];
Nucl. Phys. B 430 (1994) 319 [hep-ph/9408262].

[27] M. Laine and O. Philipsen, Nucl. Phys. B 523 (1998) 267 [hep-lat/9711022].

[28] M. Laine and O. Philipsen, Phys. Lett. B 459 (1999) 259 [hep-lat/9905004].

[29] K. Kajantie, M. Laine, J. Peisa, A. Rajantie, K. Rummukainen and M. Shaposhnikov, Phys. Rev. Lett. 79 (1997) 3130 [hep-ph/9708207].